REPORT DOCUMENTATION PAGE

AFRL-SR-BL-TR-00-

0398

1. AGENCY USE ONLY *(Leave blank)*	2. REPORT DATE	3. REPORT TYPE AND DATES COVERED
	August 3, 2000	FINAL 04/01/97 - 09/30/99

4. TITLE AND SUBTITLE
Ballistic Electron Emission Microscopy Study of Novel Quantum Objects and Electronic Defects

5. FUNDING NUMBERS
F49620-97-10247

6. AUTHOR(S)
04/01/97-09/30/98 V. Narayanamurti
10/01/98-09/30/99 J. Bowers, V. Narayanamurti

7. PERFORMING ORGANIZATION NAME(S) AND ADDRESS(ES)
04/01/97-09/30/98 University of California, Santa Barbara 93106
10/01/98-09/30/99 Harvard University as subcontract, UCSB 02138

8. PERFORMING ORGANIZATION REPORT NUMBER

9. SPONSORING/MONITORING AGENCY NAME(S) AND ADDRESS(ES)
Air Force Office of Scientific Research (AFOSR)
801 North Randolph Street
Arlington, VA 22203-1977

10. SPONSORING/MONITORING AGENCY REPORT NUMBER

11. SUPPLEMENTARY NOTES

12a. DISTRIBUTION/AVAILABILITY STATEMENT
Distribution unlimited, approved for public release.

12b. DISTRIBUTION CODE

13. ABSTRACT *(Maximum 200 words)*

Over the approximately 2 ½ year period of the above AFOSR grant, substantial progress has been made in the further development of Ballistic Electron Emission Microscopy (BEEM) as a quantitative microscopic and spectroscopic tool for the characterization of buried quantum objects and electronic defects in semiconductors. During the period of this grant, we have done the following:

i. Developed a theoretical model for the simulation of BEEM spectra. The model is compared with the experimentally obtained Second Derivative (SD) spectra for the prototypical case of $Al_xGa_{1-x}As/GaAs$ heterostructures. Quantitative numerical agreement is obtained.
ii. We have extended the modeling with Monte Carlo simulations to get detailed understanding of BEEM spectra as a function of depth below the surface.
iii. BEEM has been used for several spectroscopic studies on novel materials systems. These include observation of the splitting of the L band in GaInP due to ordering; the "local" conduction band offset of GaSb quantum 'dots' grown on GaAs; study of local electrical transport within the network of dislocations in GaN; and finally, the measurement of heterojunction band offsets in several planar heterostructures based on arsenides, phosphides and antimonides.

14. SUBJECT TERMS
Ballistic Electron Emission Microscopy (BEEM)

15. NUMBER OF PAGES

16. PRICE CODE

17. SECURITY CLASSIFICATION OF REPORT	18. SECURITY CLASSIFICATION OF THIS PAGE	19. SECURITY CLASSIFICATION OF ABSTRACT	20. LIMITATION OF ABSTRACT
UNCLASSIFIED	UNCLASSIFIED	UNCLASSIFIED	UL

TABLE OF CONTENTS

BALLISTIC ELECTRON EMISSION MICROSCOPY STUDY OF NOVEL QUANTUM OBJECTS AND ELECTRONIC DEFECTS

AFOSR Grant F49620-97-10247
Grant Period: 04/01/97 through 09/30/99

Principle Investigator: 04/01/97 through 09/30/98 ***Venkatesh Narayanamurti***
Richard A. Auhll Professor and Dean of Engineering, University of California at Santa Barbara

Principle Investigator: 10/01/98 through 09/30/99 ***John Bowers,*** UCSB
Subcontracted to Harvard University and ***Venkatesh Narayanamurti***
John A. and Elizabeth S. Armstrong Professor and Dean, Harvard University

Executive Summary

Over the approximately 2 ½ year period of the above AFOSR grant, substantial progress has been made in the further development of Ballistic Electron Emission Microscopy (BEEM) as a quantitative microscopic and spectroscopic tool for the characterization of buried quantum objects and electronic defects in semiconductors. During the period of this grant, we have done the following:

i. Developed a theoretical model for the simulation of BEEM spectra. The model is compared with the experimentally obtained Second Derivative (SD) spectra for the prototypical case of $Al_xGa_{1-x}As/GaAs$ heterostructures. Quantitative numerical agreement is obtained.

ii. We have extended the modeling with Monte Carlo simulations to get detailed understanding of BEEM spectra as a function of depth below the surface.

iii. BEEM has been used for several spectroscopic studies on novel materials systems. These include observation of the splitting of the L band in GaInP due to ordering; the "local" conduction band offset of GaSb quantum 'dots' grown on GaAs; study of local electrical transport within the network of dislocations in GaN; and finally, the measurement of heterojunction band offsets in several planar heterostructures based on arsenides, phosphides and antimonides.

The work reported here was performed primarily by M. Rubin (PhD '98), S. Bhargava (PhD '98), E.Y. Lee (Assistant Research Engineerg), M. Kozhevnikov (Research Associate), C. Zhang (Graduate Student), and H.H.Lee (Graduate Student).

I. Introduction

Ballistic Electron Emission Microscopy (BEEM) is a three-terminal modification of Scanning Tunneling Microscopy (STM) which has been widely used for the study of Metal-semiconductor (m-s) interfaces.[1,2,3] More recently [4] the Principal Investigator of this grant and his group have extensively used this technique to study semiconductor heterojunctions buried substantially below the m-s interface.

Over the last three years we have made substantial progress in developing quantitative theoretical models for BEEM and compared them with our experiments, as well as gained understanding of the scattering processes inside the semiconductor. Finally several new materials systems have been studied. This final Technical Report provides a summary of this work.

II. Scattering Models and Experiment

The original theoretical description of BEEM was based on a planar tunneling model and assumed transverse momentum conservation [2] at the m-s interface. However, until recently it was not possible to quantitatively describe the BEEM spectra anisotropy or distribution between different conduction channels for non-epitaxial systems such as Au/GaAs and Au/Si.

To analyze quantitatively the experimental data, the m-s interface-induced scattering (MSIS) model was proposed by us.[5] The authors showed that the experimental data for Au/Si and Au/GaAs systems could be fitted only by taking into account of the strong carrier scattering at the m-s interface. Recently, to quantitatively analyze the electron scattering at the m-s interface, this model was modified to include anisotropy of the electron effective mass, the energy dependence of the electron mfp in the metal base, and finite temperature.[6] In this model, the conduction process is described by carrier multivalley transport with corrections due to the scattering at the m-s interface, which depends on the m-s scattering probability. When interface scattering is considered, the BEEM current is given by [6]

$$I_c = eA\sum_{\vec{k}^t} F_{\perp}^{t}(\vec{k}^t)T^{V_t}(\vec{k}^t,\vec{k}^b)D(\vec{k}^b)$$
$$\times\left[\left(1-\sum_f P_{\vec{k}^b,\vec{k}^f}\right)T^{i}(\vec{k}^b,\vec{k}^{sb})T^{h}(\vec{k}^{sb})+\sum_f P_{\vec{k}^b,\vec{k}^f}T^{i}(\vec{k}^b,\vec{k}^{sb})T^{h}(\vec{k}^{sb})\right] \quad (2)$$

where $P_{\vec{k}^b,\vec{k}^f}$ is the probability for the electron with the wavevector $\vec{k}^b$ to be scattered into the state labeled by the wavevector $\vec{k}^f$. The first and second terms in brackets correspond to electrons that are not scattered and that are scattered, respectively.

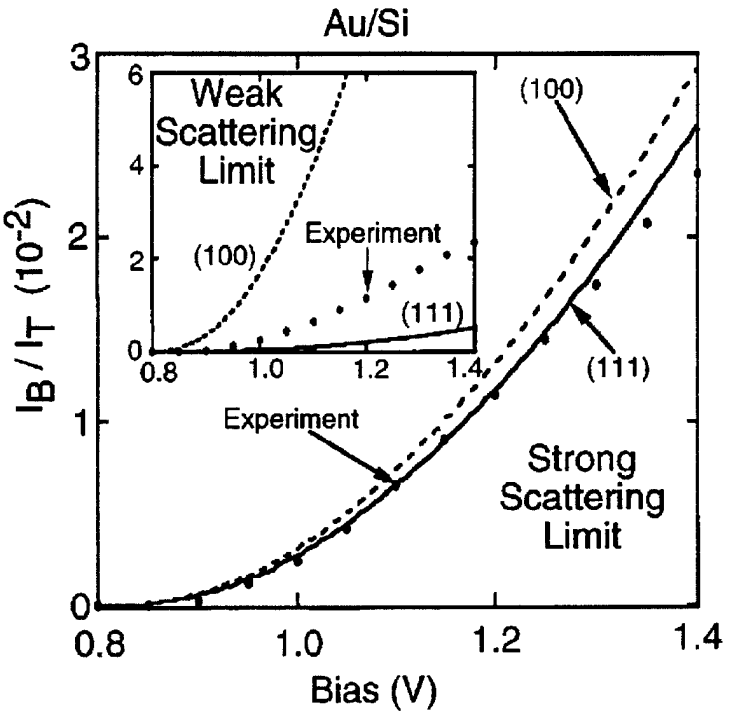

Fig. 1. Comparison of the calculation in the strong scattering limit for Au/Si(100) (dashed line) and Au/Si(111) (solid line) with the experimental results for Au/Si. These measurements were made on Au/Si(111) but measurements for Au/Si(100) are very similar to those for Au/Si(111). The inset compares the calculation in the weak scattering limit to the same experimental results (from D. L. Smith, E. Y. Lee, and V. Narayanamurti, Phys. Rev. Lett. 80, 2433 (1998)).

In this model, if scattering at the m-s interface is strong, the injected electron flux distribution is redistributed and valleys with zero interface transverse wavevector at their energy minimum are not preferentially weighted. Instead the weighting goes like the density of final states for the scattering process. Fig. 1 compares the calculated BEEM current in the strong and in the weak scattering limits for Au/Si with the experimental results. One can see that the experimental data can be described adequately without fitting parameters only in the strong scattering limit. In BEEM on Au/GaAs, the calculated Γ channel contribution is much larger than the L channel contribution to the collector current in the weak scattering limit, whereas the L channel contribution is much larger than the Γ channel contribution in the strong scattering limit (see Fig. 2). Scaled threshold shapes are similar in the weak and strong scattering limits for conduction band valleys that make a circular projection on the interface plane, such as Γ and X valleys. For conduction band valleys that make a strongly anisotropic projection on the interface plane, such as the L valleys of GaAs(100), the calculated L channel currents have significantly different threshold shapes in the two limits, as shown in Fig. 3. When the calculations are done in a spherical approximation, the threshold shapes are similar in the two limits and look like the result of the more complete anisotropic model in the strong scattering limit.

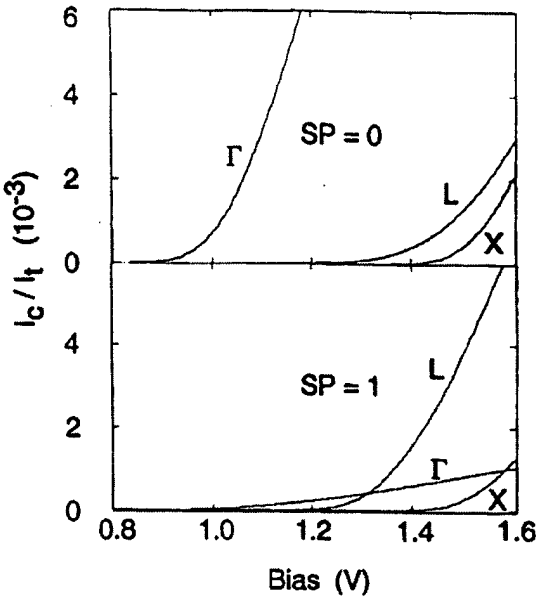

Fig. 2. Calculated ratio of collector to tunneling current as a function of bias for the three conduction band channels of Au/GaAs(100) in the weak scattering limit (upper panel) and in the strong scattering limit (lower panel) (from D. L. Smith, M. Kozhevnikov, E.Y. Lee and V. Narayanamurti, Phys. Rev. B61, 13914 (2000)).

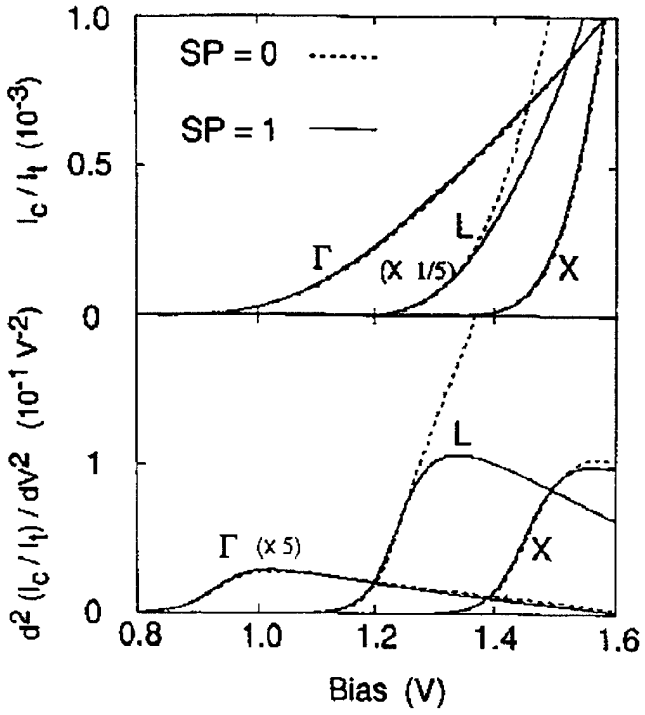

Fig. 3. Scaled ratio of collector to tunneling current (upper panel) and scaled second voltage derivative of the ratio of collector to tunneling current (lower panel) as a function of bias for the three conduction band channels of Au/GaAs(100). The scaling factors for all the valleys were chosen so that the currents for two limits overlap well in the near threshold region. The strong scattering limit results (solid lines) are as calculated and the weak scattering limit results (dashed lines) are scaled by: Γ channel, divide by 31; *L* channel, multiply by 4.5; *X* channel, divide by 1.7 (from D. L. Smith, M. Kozhevnikov, E.Y. Lee and V. Narayanamurti, Phys. Rev. B61, 13914 (2000)).

Recently, the electron scattering at the metal-semiconductor interface was studied experimentally by us in the Au/GaAs/$Al_xGa_{1-x}As$ system by using second derivative (SD) BEEM spectroscopy.[7] The SD-BEEM spectrum is proportional to the heterostructure transmission coefficient, and is particularly useful both for separating the contributions from various conduction band channels and for analyzing the threshold shapes. The analysis of the spectral shape is more effective than just the BEEM current magnitude because the absolute value of the BEEM current could be scaled by the fluctuations in both the metal layer and semiconductor epilayer thickness. In GaAs, conduction bands with both zero and large interface parallel wavevector coexist in the same material. Thus direct and indirect transport channels can be investigated in the same sample. The observed SD-BEEM spectral shape shows obvious deviation from the calculations that assume transverse momentum conservation. In Fig. 4, we compare the calculated (dashed lines) collector current and its second voltage derivatives with the corresponding measured quantities (solid lines) for a Au/GaAs sample at room temperature. The SD spectrum was extracted from the experimental BEEM spectrum in Fig. 4(a) by numerical differentiation with a 10 meV window, as shown in Fig. 4(b).

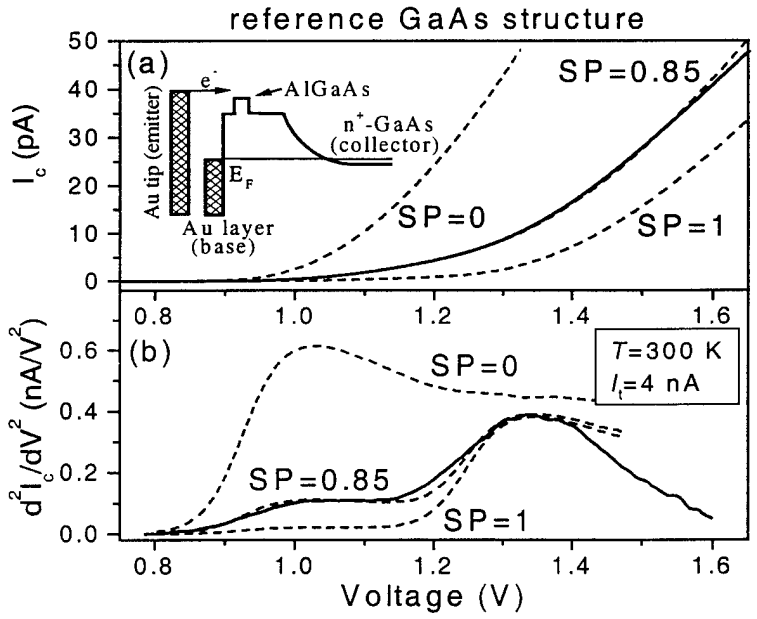

Fig.4 The room-temperature BEEM (a) and SD-BEEM (b) spectra of the 1 μm undoped GaAs layer grown on n^+ GaAs substrate. The MSIS model calculations (dashed lines) are also presented for three values of SP, the electron scattering probability at the m-s interface. The inset in (a) shows a schematic band diagram of the samples under study (from M. Kozhevnikov, V. Narayanamurti, C. Zheng, Y.-J. Chiu, and D. L. Smith, Phys. Rev. Lett. **82**, 3677 (1999)).

The probability of electron scattering at the m-s interface (SP) was adjusted to fit the SD-BEEM spectra. The SD-BEEM spectra clearly separate the contributions from Γ and *L* electrons; thus, the weighting of the relative Γ and *L* channel contribution is a sensitive test of the model. The best fit to the SD-BEEM spectrum gives an 85% probability for electron scattering at the m-s interface. For comparison, theoretical curves for the cases without scattering and with 100% scattering are also shown. The measured relative contribution of the L-electrons is different than that calculated for the *L* channel in the weak scattering limit. Specifically, the *L*-electron collector current is found to be the strongest one, whereas, assuming transverse momentum conservation, the contribution of the

L band (which does not project to the zone center of the interface Brillouin zone) can give only a small BEEM current onset. The Γ and *L* channel contributions are included in the calculation but the *X* channel contribution is not included. In this experimental structure, the absence of the *X* conduction minimum contribution at room temperature is due to the image potential-induced strong electron scattering in the spacer between the metallurgical m-s interface and the maximum of the barrier height. Fig. 5 presents the MSIS model fits to the BEEM and SD-BEEM spectra for a number of Au/GaAs/$Al_xGa_{1-x}As$ single barrier structures. In this case, the best fits are obtained with the scattering probability at the m-s interface varying between 85% and 92% among these samples. This small variation in the scattering parameter indicates that our diode fabrication procedure is reproducible and results in approximately the same quality of the m-s interface.

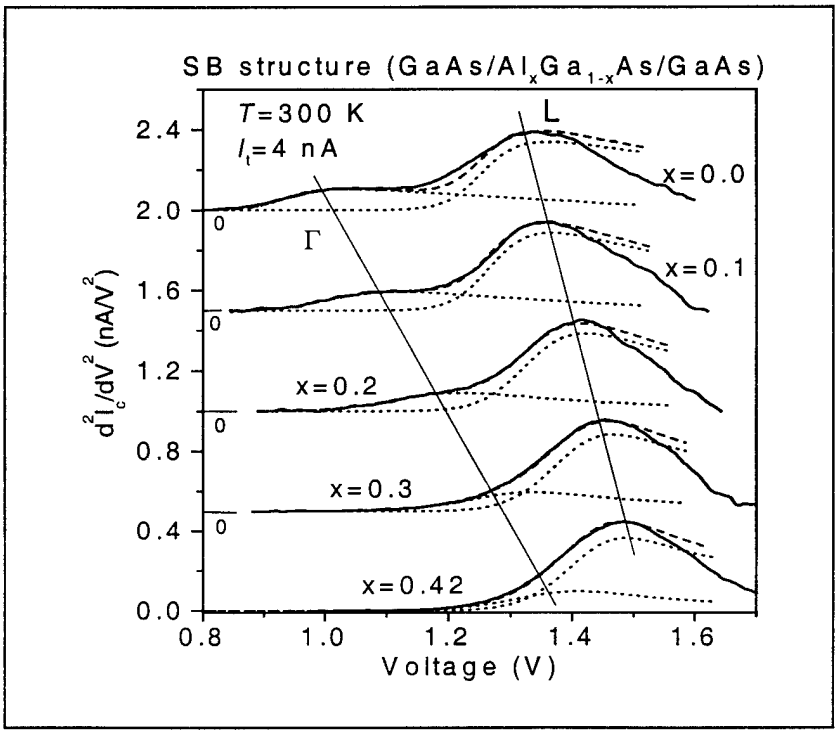

Fig. 5. Room-temperature SD-BEEM spectra for five different Al compositions (solid lines). For clarity, the SD-BEEM spectra are shifted along the vertical axis. Thin solid lines are eye-guides for the peaks position development. The MSIS model calculations are also presented. The model calculations show the separate Γ and L valley contributions (dotted lines) and their sum (dashed lines) (from M. Kozhevnikov, V. Narayanamurti, C. Zheng, Y.-J. Chiu, and D. L. Smith, Phys. Rev. Lett. **82**, 3677 (1999)).

In summary, through the combination of SD-BEEM spectroscopy and theoretical modeling, which takes into account the parallel momentum non-conversation, we are able to quantitatively describe BEEM data. This ability clearly makes BEEM a more useful spectroscopic and microscopic tool.

III. BEEM Depth resolution

The hot electron transport in BEEM experiments can be considered to be ballistic only with certain restrictions. The real picture is certainly different because of consecutive scattering processes in the metal base film, at the metal/semiconductor interface and in the semiconductor itself. Even for the case of a perfectly clean device and extremely low temperatures, the carrier mean free path is usually comparable with the device thickness. Therefore, the ballistic description of the electron transport is restricted to layers close to the surface. As a consequence, BEEM can be characterized by its depth resolution.

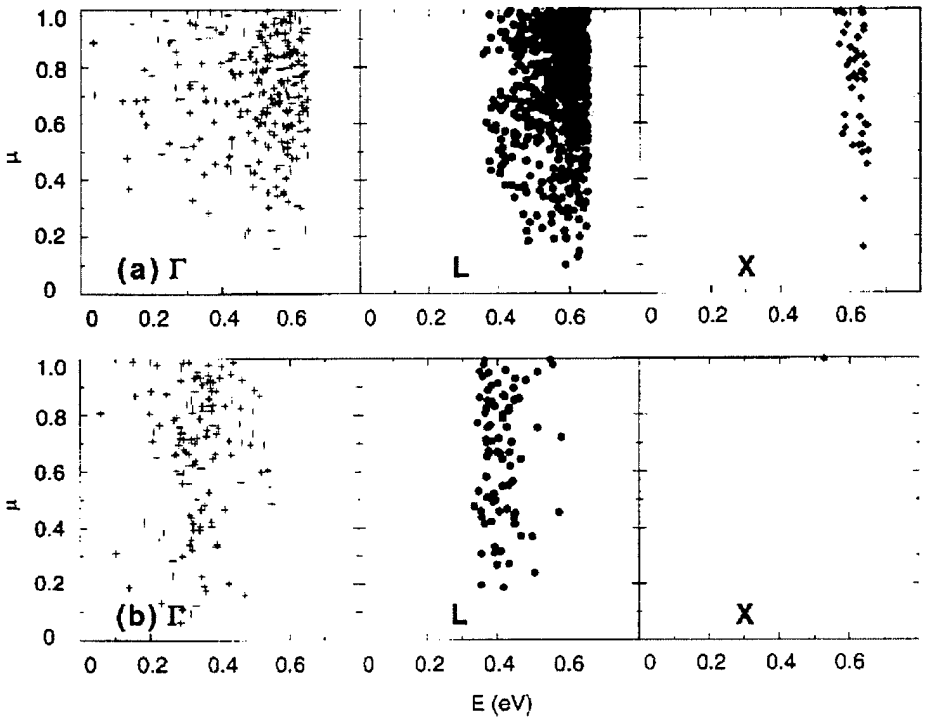

Fig. 6. For the populations of the electrons in GaAs resulting from a BEEM experiment of Au-GaAs, the energy and angular distributions are shown. The *y* axis is the cosine, denoted by μ, of the angles of the velocities of the electrons with respect to the interface normal and the *x* axis is the kinetic energy *E* of the electrons with respect to the Γ-valley minimum. The condition is the strong scattering limit of SLN theory at 300 K and at a bias of 1.53 V. Initially, 1000 electrons are injected at the Au-GaAs interface. (a) The initial electron distributions of Γ- (left panel and crosses), *L*- (middle panel and circles), and *X*- (right panel and diamonds) valley electrons at the Au-GaAs interface. (b) The distributions at 600 Å below the Au-GaAs interface (from E. Y. Lee, Phys. Rev. **59,** 15332 (1999)).

Monte Carlo simulations [8] of electron transport in the Γ, L and X valleys of GaAs were performed using the MSIS model.[5] With increasing object depth beneath the Au/GaAs interface, the Monte Carlo simulations predict (1) significant cooling of hot electrons, on the order of ~3meV/nm at 1.5 eV, and (2) significant redistribution of electrons among the conduction bands (see Fig. 6). In order to show experimentally that scattering inside the semiconductor structure affects the BEEM spectra, in Ref. 7 we compared the BEEM spectra for several pairs of Au/GaAs/AlGaAs single barrier (SB) samples with the same SB composition but with different cap thickness of 50 Å and 300 Å. The obtained SD-BEEM spectra of the GaAs/$Al_{0.2}Ga_{0.8}As$/GaAs SB samples are shown in Fig. 7 for T=85K and 300K (these data are representative for all samples pairs).

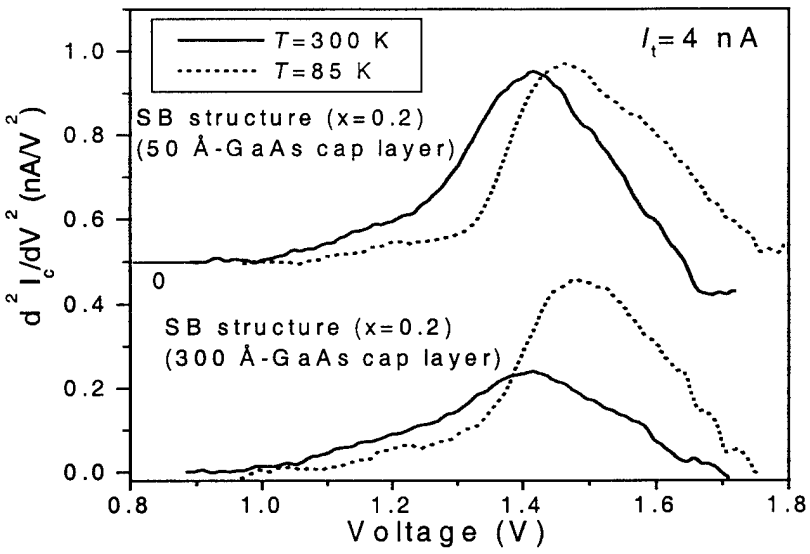

Fig. 7. SD-BEEM spectra for GaAs/$Al_{0.2}Ga_{0.8}As$/GaAs SB samples with 50 Å and 300 Å GaAs cap layers, taken at *T*=300 K (solid curves) and *T*=85 K (dotted curves). For clarity, the spectra are shifted along the vertical axis (adopted from M. Kozhevnikov, V. Narayanamurti, C. Zheng, Y.-J. Chiu, and D. L. Smith, Phys. Rev. Lett. **82**, 3677 (1999)).

Since the expected mfp lengths for the Γ, L and X electrons at T=300K are ~1000 Å, ~100 Å and ~10 Å, respectively, [9] manipulations with the heterostructure thickness in the range of 100-300 Å should affect mainly the L-electrons contribution to the BEEM current (the effective heterostructure thickness, that will affect the BEEM current collection, is the combined thickness of the GaAs cap layer and the SB layer.) Indeed, as one can see from Fig. 7, the L-electrons contribution for the sample with 300 Å-cap layer (with the SB thickness of 50 Å, the total effective heterostructure thickness is ~350A) is reduced by factor of 3 as compared with the 50 Å-cap layer sample (the total effective thickness of ~100 Å), whereas the Γ contribution has remained intact. As the temperature decreases from 300 K to 85 K, in addition to the spectrum shift expected from the temperature dependence of the energy gap, a strong increase of the signal is observed for the *L*-electrons in the SB sample with the 300 Å-cap layer, whereas the SD-BEEM spectral shape remains essentially the same for the SB sample with the 50 Å-cap layer. These experimental results are in agreement with the expected increase in the mfp of the electrons with the decreasing temperature. As the temperature decreases from 300 K to 85 K, the calculated mfp near the energy threshold increases from ~1000 Å to ~1500 Å for Γ electrons and from ~100 Å to ~300 Å for the *L* electrons.[9] The X-electrons contribution is completely obscured in the room-temperature BEEM spectra presented in Fig. 7 due to their cooling-induced effective scattering in the GaAs cap layer. Indeed, the X-electrons mfp (~10 Å at T=300 K and ~30 Å at T=85 K) is shorter than the effective heterostructure thickness for all samples (≥100 Å). Thus, while the initial electron distribution among the conduction bands of the semiconductor is specified by transport through the metal base layer and by the m-s interface scattering, further electron transport is governed by the difference in the electron mean-free-path (mfp) length for the Γ, L and X electrons. In imaging the buried semiconductor structures, the mfp length (in the case of GaAs-based structures, the mfp length of Γ-electrons as the longest one) will determine the depth resolution of BEEM. It implies that the BEEM contrast will be not enough to resolve a semiconductor structure buried deeper than ~1000Å (mfp of the Γ-

electrons). Therefore, as the heterostructure, characterized by several transport channels, is buried deeper, the information about these conduction channels is gradually gone, starting from the transport channel with the shortest electron mfp length.

Lee et al [10] have performed Monte Carlo simulations of the transport of electrons injected into the Γ valley of GaAs for BEEM imaging and spatially resolved spectroscopy of model quantum dots (QD) and quantum wires (QW) buried beneath the Au/GaAs interface. For Monte Carlo simulations, a modified BK model was used, with the buried object forming a local barrier for the electron transmission (such as AlSb and GaSb dot grown on GaAs). The collection plane was located at 2000Å below the Au/GaAs interface, and the QD (QW) was modeled as a thin disk 300Å in diameter (a thin 300Åwide stripe), which specularly scatters electrons of all energies. Fig. 8 shows the calculated BEEM current as a function of x, a lateral displacement between the STM tip and the center of the buried dot (wire), for three depths of the QD (QW) from the Au/GaAs interface. One can see that the BEEM contrast decreases with the depth of the object. At a depth of 600Å, a QD is hardly detectable by BEEM whereas the QW still shows significant contrast, due to the added dimension. In addition, it was shown that due to an interplay between a geometric filtering effect and the role of the electron-phonon scattering (assuming electron transverse momentum conservation at the m-s interface), there is a range of optimum depths for the sharpest crystal momentum and energy distribution of the electrons incident upon the buried structure.

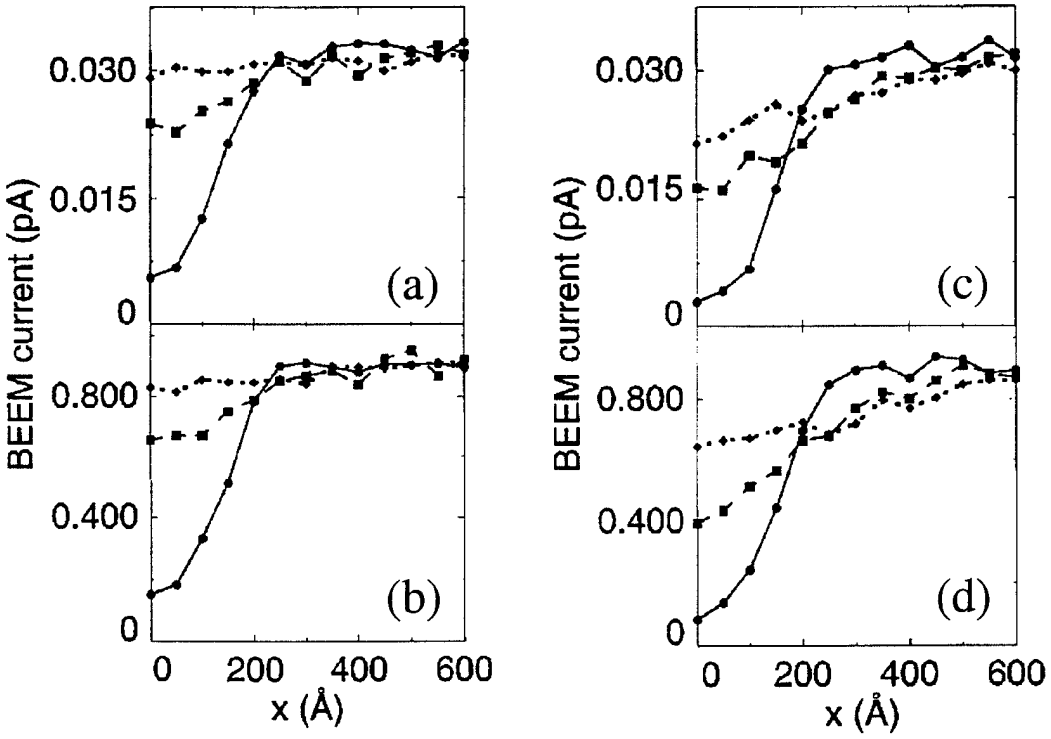

Fig. 8. The BEEM current as a function of lateral displacement at a tip-to-sample bias of 1 V (a) and 1.25 V (b) for a perfectly reflecting quantum dot 300 Å in diameter, and at a
tip-to-sample bias of 1 V (c) and 1.25 V (d) for a perfectly reflecting 300Å wide quantum wire. The lines are drawn as a guide for the eye. In all cases, the solid line (circle) is for d=100 Å, the dashed line (square) is for d=300 Å, and the dotted line (diamond) is for d=600 Å (adopted from E. Y. Lee, V. Narayanamurti, and D. L. Smith, Phys. Rev. **B55,** R16033 (1997)).

As an example of BEEM imaging of deeply buried localized objects, a study of misfit dislocations at the $In_xGa_{1-x}As/GaAs$ interface buried 400-700 Å below the m-s interface was conducted in our laboratory.[9,11,12] The cross-hatch misfit dislocation network in InGaAs/GaAs was ideally suited for BEEM as the dislocation core beneath the surface gives rise to a perturbation at the surface easily visible by AFM or STM. Samples consist of InGaAs of different thickness grown on (001) GaAs substrates and were designed such that the dislocations will exist (In concentrations of x=0.15-0.3 and InGaAs thickness of d=400-750Å were examined).[12] Simultaneous STM and BEEM imaging, shown in Fig. 9, revealed a decrease in the BEEM current directly associated with the cross-hatch pattern in the STM.

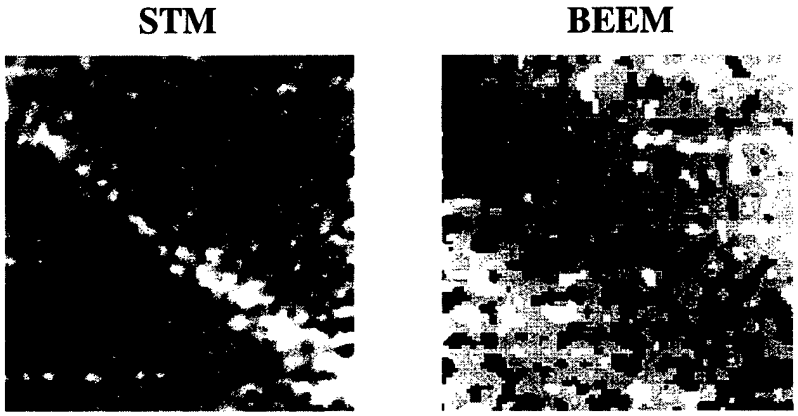

Fig. 9. 1μ×1μ STM (left) and BEEM (right) images of InGaAs/GaAs heterostructure (x=0.2, d=600Å). The STM image shows the growth perturbation caused by the dislocation core. The BEEM image shows the decrease in current at the presence of the cross-hatch (from S. Bhargava, Ph.D. dissertation, University of California at Santa Barbara, August 1998).

The minimum in the BEEM current, through analysis of line scans, was found to be shifted ~400 Å from the maximum of the STM image, indicating that the loss in BEEM current is not simply a surface affect, but one that arises from the dislocation core located ~600Å beneath the surface (see Fig. 10). This is in agreement with the theory that the dislocation core comes to the surface not along the growth direction, but along the glide plane (111), which is 54.7° off of the (100) direction. Monte Carlo calculations were used to understand the mechanism responsible for this decrease [12]. The simulation of the charged model fit closest to the experimental data suggesting that backscattering off of line charges to the metal base is responsible for the loss in BEEM current.

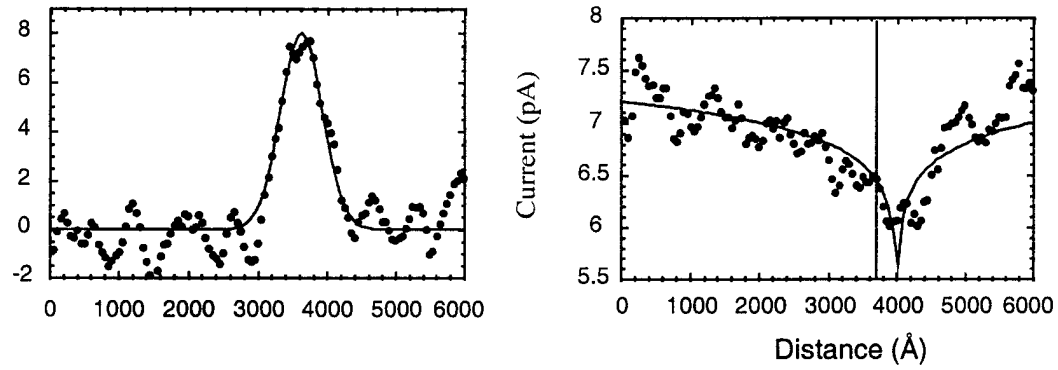

Fig. 10. STM (left) and BEEM (right) linescanes taken over dislocation images. The STM linescanes show a Gaussian peak while the BEEM linescanes show a drop in the BEEM current shifted from the peak in the STM image (from S. Bhargava, Ph.D. dissertation, University of California at Santa Barbara, August 1998).

IV. GaInP

In the past decade, spontaneous CuPt ordering of many III-V alloys has been widely observed in vapor phase growth on (001) substrates. In $GaInP_2$, extensive theoretical [13,14] and experimental [15] work has been carried out to study the effect of the ordering-induced reduction of the crystal symmetry on the structural, optical and transport properties of the ordered material. Ordering induced changes in the band structure of $GaInP_2$ are important for its application in advanced solar cells with very high conversion efficiency, for potential band-gap engineering and for fundamental studies of atomic ordering.

Perfectly ordered material has not been observed. The electronic states of a partially ordered structure can be interpolated from those of the totally disordered and the perfectly ordered semiconductor.[14] The degree of ordering is usually described by the ordering parameter η, where $E_g(\eta)=E_g(\eta=0)-\eta^2\Delta E_g(\eta=1)$, with $\eta=0$ and $\eta=1$ to describe perfectly disordered and perfectly ordered material, respectively. $E_g(\eta=0)$, the bandgap of disordered GaInP, is 2.01 eV at low temperature [16] and $\Delta E_g(\eta=1)$, the maximum bandgap reduction for perfectly ordered GaInP, is 0.47 eV.[17] In the most ordered $GaInP_2$ structures, the highest ordering parameter $\eta \sim 0.6$, [18] and the degree of ordering is nonuniform on the local scale.

To characterize the structural and electronic properties of $GaInP_2$, we have applied the BEEM technique.[19, 20] The undoped GaAs/$GaInP_2$ structures on n^+- and p^+- GaAs substrates were grown by metal organic chemical vapor deposition (MOCVD), at T_g = 650°C. The structures consist of a 500 Å undoped GaAs buffer layer, a 1 μm $GaInP_2$ and a 50Å GaAs cap layer. A detailed analysis is presented here for the $GaInP_2$ samples grown on a (511) GaAs substrate and on a (001) GaAs substrate misoriented 6° toward $[111]_B$. From the low-temperature photoluminescence, the bandgap energy (after correction on the exciton binding energy) is ~2.00 eV for $GaInP_2$ grown on a (511) GaAs substrate and ~1.88 eV for $GaInP_2$ grown on a $6°[111]_B$-(001) GaAs substrate. Therefore, we conclude that the $GaInP_2$ layer grown on a (511) GaAs substrate is highly disordered (hereafter,

disordered $GaInP_2$) and the $GaInP_2$ grown on a (001) GaAs substrate misoriented 6° toward $[111]_B$ is highly ordered, $\eta \sim 0.5$ (hereafter, ordered $GaInP_2$).[14]

Fig. 10 shows room-temperature 1 μm × 1 μm STM images of the disordered (a) and ordered (b) $GaInP_2$ layer grown on n^+-GaAs substrates. One can see that the surface of ordered material forms [110] –oriented steps. For ordered $GaInP_2$ grown on misoriented substrates, the [110] steps are usually observed to form only single CuPt variant.[21,22] For disordered $GaInP_2$, the surface is found to be much flatter than that of ordered $GaInP_2$. The complementary BEEM images are also shown in Fig. 10. The observed contrast of the BEEM image for the ordered $GaInP_2$ sample is in direct correlation with the surface morphology, indicating high sensitivity and high spatial resolution of the BEEM technique.

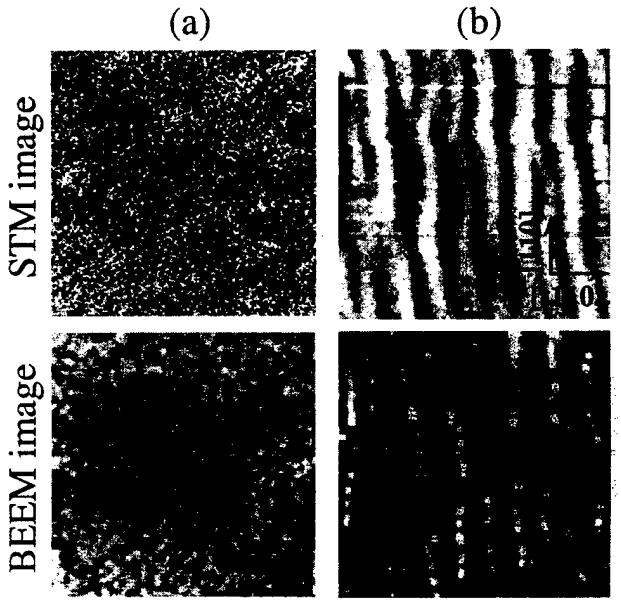

Fig. 10. Room-temperature 1 μm × 1 μm STM image (top) and BEEM image (bottom) of GaAs/$GaInP_2$ layer grown by MOCVD on (a) (511) n-GaAs substrate, (b) on n-GaAs substrate misoriented by 6° to $[111]_B$. A tip bias is -1.7 V and a tunnel current is 4 nA (from M. Kozhevnikov, V. Narayanamurti, A. Mascarenhas, Y. Zhang, J.M. Olson, and D. L. Smith, Appl. Phys. Lett 75, 1128 (1999)).

To study the heterostructure transmission coefficient, we analyze the second voltage derivative (SD) of the BEEM spectra rather than the original BEEM spectra.[20] Fig. 11 shows the SD-BEEM spectra obtained from the experimental BEEM data by numerical differentiation with a 10 meV window. We associate two clearly pronounced features in the 77K SD-BEEM spectra of disordered $GaInP_2$ with the Γ and L conduction minima contribution in $GaInP_2$. Theoretical fits to the SD-BEEM spectrum for the disordered $GaInP_2$ sample, using the MSIS model,[5,7] are shown in Fig. 11 by the dashed line. The MSIS model-fit describes the experimental BEEM spectrum reasonably well, giving ~90% probability of the electron scattering at the m-s interface, similar to our previous results for GaAs/AlGaAs structures.[7] The absence of a contribution from the X conduction minimum is due to strong X-electron attenuation in the GaAs cap layer.[7]

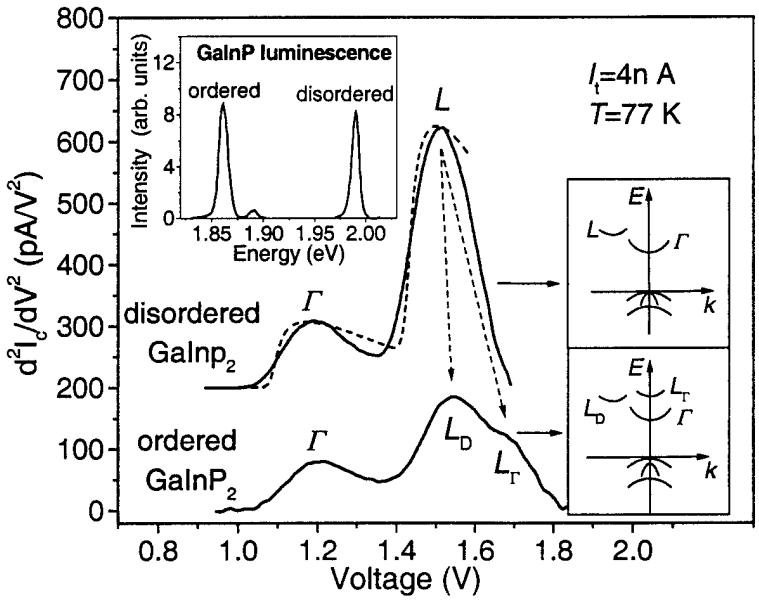

Fig. 11. SD-BEEM spectra for two GaAs/$GaInP_2$ (ordered and disordered) samples with 50 Å GaAs cap layers, taken at $T = 77$ K. For clarity, the spectra are shifted along the vertical axis. The MSIS model calculations are also presented (dashed line). The top inset shows the photoluminescence spectra for both ordered and disordered GaInP samples, whereas two bottom insets show the schematic of the GaInP band structure (from M. Kozhevnikov, V. Narayanamurti, A. Mascarenhas, Y. Zhang, J.M. Olson, and D. L. Smith, Appl. Phys. Lett 75, 1128 (1999)).

The SD-BEEM spectrum of the ordered $GaInP_2$ sample presented in Fig. 11 show a very important difference from that of the disordered $GaInP_2$. Namely, we observe two high-energy peaks instead of one peak in disordered $GaInP_2$. We assign both high-energy peaks to be associated with the L valley contribution. In CuPt-type ordered $GaInP_2$, one of the four L valleys folds onto the $\overline{\Gamma}$ point (hereafter L_Γ), and the other three are folded onto the $\overline{D}$ point (hereafter L_D). A strong repulsion between the Γ valley and the folded L_Γ valley results in the bandgap reduction and in the increase of the Γ- L_Γ separation, while the energetic position of the L_D remains almost the same. Therefore, we conclude that the two observed high-energy peaks for the ordered sample are the contribution of the L valleys that are split due to ordering.

The "folded" zone-edge bands were observed experimentally in electro-reflectance[23] and Raman spectroscopy[24] measurements. In the recently reported electro-absorption experiments on ordered $GaInP_2$ ($\eta \approx 0.45$)[25], an additional feature was observed at ~ 0.48 eV above the fundamental bandgap transition, and this feature was attributed to the back folded L conduction band. As the ordering decreases, this peak shifts to lower energies, with an asymptotic value of ~ 0.33 eV above the fundamental bandgap transition for a totally disordered sample. In Refs.[23-25], due to the selection rules, only the contribution from the L valley folded onto the $\overline{\Gamma}$ point was observed. In contrast, we observe the contribution from all L valleys and, as a consequence, can measure directly the Γ-L separation in disordered $GaInP_2$ as well as the ordering-induced L valley splitting in ordered $GaInP_2$. According to our results, $\Delta(\Gamma\text{-}L) \cong 0.35$ eV for a disordered sample, $\Delta(\Gamma\text{-}L_\Gamma) \cong 0.47$ eV and $\Delta(L_\Gamma\text{-}L_D) \cong 0.13$ eV for an ordered sample. These results are in a good agreement with the theoretical predictions. Indeed, as pointed out by Zunger, [26] it is possible to obtain the dependencies

$\Delta(\Gamma\text{-}L_\Gamma) = \Delta(\Gamma\text{-}L)_{\eta=0} + 0.5\eta^2$ and $\Delta(\Gamma\text{-}L)_{\eta=0}$=0.35 from our experiment, $\Delta(\Gamma\text{-}L_\Gamma) \cong 0.475$ eV and $\Delta(L_\Gamma\text{-}L_D) \cong 0.11$ eV.

This then, is an example of obtaining entirely new information on band structure of a new material, which heretofore was not possible.

V. GaSb Quantum Dots Grown on GaAs

GaSb self assembled quantum dots grown by MBE on GaAs exhibit a staggered (type II) band lineup with a potential barrier in the conduction band.[28-30] Therefore, electron-hole recombination in these structures is spatially indirect, so that optical measurements do not provide adequate information about the conduction band offset between the GaSb dots and GaAs. Along with that, traditional transport methods cannot measure this local band offset because of the small (~50 nm) lateral dot size, and any offset measurement would average over areas with and without dots. In BEEM, however, carriers are locally injected into semiconductor structures to spectroscopically probe buried interfaces on a nanometer scale.

Figure 12 shows STM and BEEM images of a single, GaAs capped, GaSb dot. In the STM image, a roughly circular feature ~ 50 nm in diameter and ~ 5 nm tall, marks the lateral position of the buried dot. The area in the BEEM image aligned with the dot profile in STM is darker than the surrounding region, implying that the BEEM current through the dot is reduced due to electrons reflection off the dot's potential barrier. The height of this barrier, i.e. the local band offset, can be extracted from the changes in BEEM spectra between the on and off cases. The on dot and off dot BEEM spectra of several dots were fitted by using a modified Bell-Kaiser planar tunneling model,[31] giving a local conduction band offset for GaSb dots on GaAs of 0.08±0.02 eV. For details of this study, see Ref.[32].

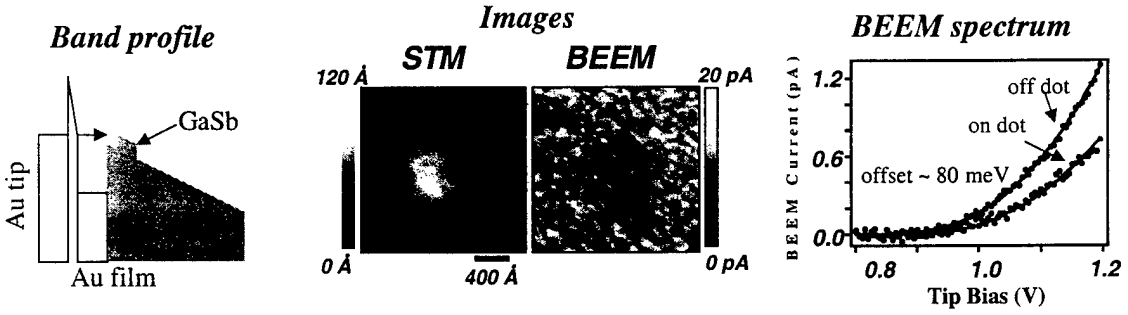

Fig. 12. (from left to right) Schematic of band profile, STM and BEEM inages and characteristic BEEM spectra for GaSb/GaAs self-assembled single quantum dots (from M.E. Rubin, H.-R. Blank, M.A. Chin, H. Kroemer, V. Narayanamurti, Physica **E2**, 682 (1998)).

VI. GaN

Although GaN exhibits high-efficiency optical performance despite its extremely high dislocation densities,[33] the dislocations are very likely to have significant electrical and structural impact on high-power electronic devices.

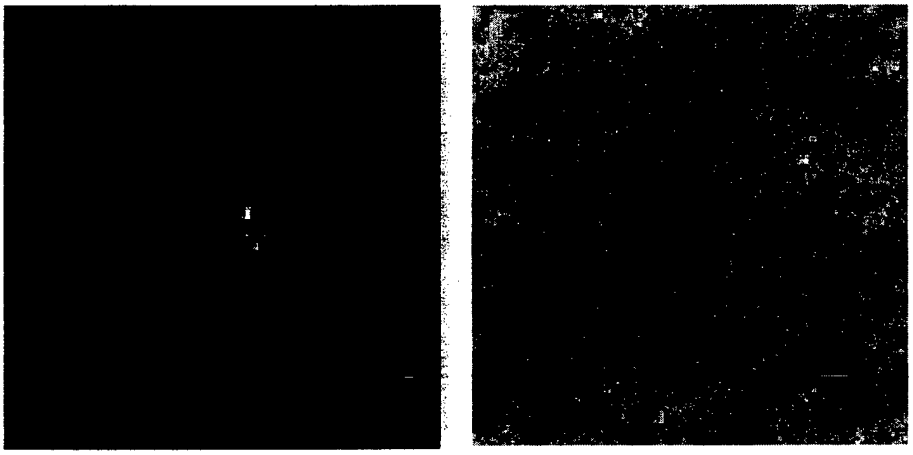

Fig. 13. Collector current image (left) and simultaneously taken STM image (right) of the 70Å Au cap layer of a 2500Å x 2500Å area (I_T = 1nA, V_T = -1.8V). The small high-current area (~500pA,bright spot) surrounded by areas with zero collector current (< 0.2pA) shown in (a) is typical for the investigated GaN-films. The Au layer (right) exhibits a pit (dark) at the location of the high-current area (bright spot (left)) (from E. Brazel, M.A. Chin, and V. Narayanamurti, Appl. Phys. Lett. **74** (16), 2367 (1999)).

The recent study of Brazel et al [34] has revealed high BEEM current densities and low effective Schottky barrier heights in small localized areas around dislocations with a screw component. The GaN-films used in that study were grown by metal organic vapor deposition (MOCVD) at atmospheric pressure. For these measurements unintentionally doped, n-type GaN-films of thicknesses ranging from 1μm up to 3μm were deposited on c-plane sapphire substrates. Fig. 13 (left) shows a typical collector current distribution for the MOCVD-grown GaN films deposited on c-plane sapphire substrates. From most parts of the sample no collector current was detectable (dark area), and only in small localized spots, like the shown light area, high collector currents could be observed. In this representative case, the measured current was ~500 pA, which is half of the injected 1nA tunneling current. To localize the high current areas on the sample surface and possibly correlate them with surface features, images of the current distribution and the topography were taken simultaneously. Fig. 13 (right) shows the STM image of the Au cap-layer, which corresponds to the collector current image in Fig. 13 (left). The 70 Å thick Au-layer exhibits a ~500 Å wide pit at exactly the same position of the high current area in the collector current image. An AFM-image taken of the same sample shows several of these pits that represents the surface terminations of mixed and pure screw dislocations. Thus, it was concluded that the high BEEM current areas are located at dislocations with screw character. To get information about the Schottky barrier heights, the BEEM spectroscopy in both high and low currents areas was carried out. The low current areas do not show any measurable collector current, whereas for the high current areas, we have found barrier heights in the range from ~0.3 eV up to ~0.95 eV.

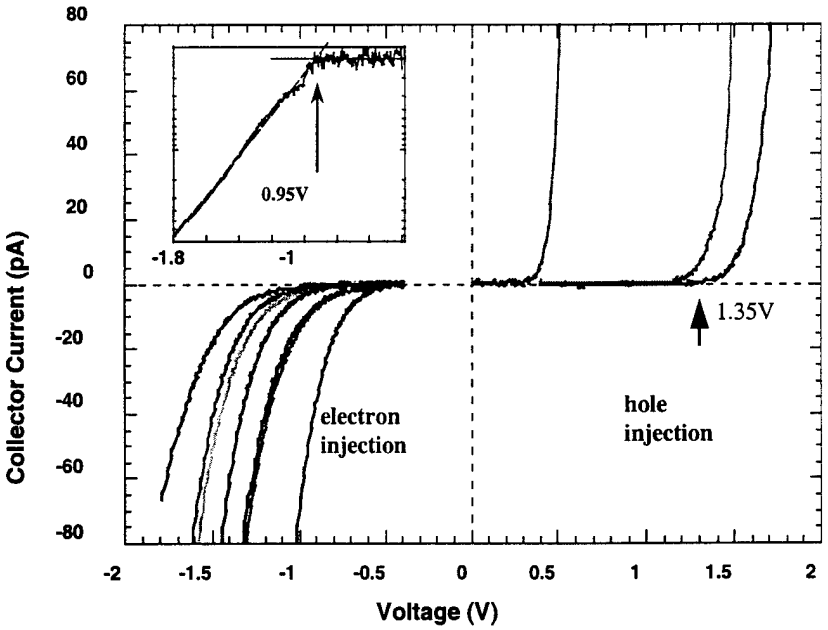

Fig. 14. I_C-V_T spectra for both, electron and hole injection, respecively. Log-plots like the one shown in the inset were used to approximately determine the threshold voltage necessary for current injection into the high-current areas (from E. Brazel, M.A. Chin, and V. Narayanamurti, Appl. Phys. Lett. 74 (16), 2367 (1999)).

The threshold values vary within one high-current area and from area to area. In addition, it was possible to reverse the tunneling voltage and inject holes into the very same high current areas as well, with the observed threshold energy of ~0.3 eV to 1.3 eV, as shown in Fig. 14. The observed thresholds for carrier injection do not seem to be typical Schottky barriers, but rather capturing barriers of trap states in the vicinity of the dislocations. These results definitely suggest that acceptor- and donor-like trap states coexist in the same area, and are being filled during carrier injection into the GaN. The maximum threshold energies observed for electrons (0.95 eV) and holes (1.3 eV) add up to 2.25 eV, remarkably close to the parasitic yellow luminescence commonly observed in GaN. In the future, we plan to conduct more experiments to answer the question whether the same electronic states, which are causing the high current densities are also responsible for the yellow luminescence.

VII. Band Offsets in Other Systems

Recently, BEEM spectroscopy has been successfully applied to determine the conduction band offset between AlInGaAs strained layer (active layer in 850 nm vertical cavity lasers) and a AlGaAs barrier located beneath the surface.[35] Also, BEEM spectroscopy has been used to study both the conduction and valence band offsets between InAs and AlAsSb at T = 77 K and T = 300 K.[36] It was found that with the addition of As to AlSb, the conduction band offset between InAs and AlAsSb decreases despite the increase in the bandgap. The resulting decrease in the valence band position causes the InAs/AlAsSb band lineup to change from a staggered (type II) to a straddling (type I).

References

1. L. D. Bell and W. J. Kaiser, Phys. Rev. Lett. 61, 2368 (1988).

2. M. Prietsch, Phys. Rep. 253, 163 (1995).

3. L. D. Bell and W. J. Kaiser, Annu. Rev. Mater. Sci. 26, 189 (1996).

4. For review, see, e.g., V. Narayanamurti, Sci. Rep. Res. Inst. Tokohu Univ. A, Phys. Chem. Metall. 44, 165 (1997).

5. D. L. Smith, E. Y. Lee, and V. Narayanamurti, Phys. Rev. Lett. **80,** 2433 (1998).

6. D. L. Smith, M. Kozhevnikov, E. Y. Lee, and V. Narayanamurti, Phys. Rev. B **61,** 13914 (2000).

7. M. Kozhevnikov, V. Narayanamurti, C. Zheng, Y.-J. Chiu, and D. L. Smith, Phys. Rev. Lett. **82,** 3677 (1999).

8. E. Y. Lee, Phys. Rev. **59,** 15332 (1999).

9. E. Y. Lee, S. Bhargava, M. A. Chin, and V. Narayanamurti, J. Vac. Sci. Technol. A **15,** 1351 (1997).

10. E. Y. Lee, V. Narayanamurti, and D. L. Smith, Phys. Rev. B **55,** R16033 (1997).

11. E. Y. Lee, S. Bhargava, K. Pond, K. Luo, M. A. Chin, and V. Narayanamurti, Appl. Phys. Lett. **69,** 940 (1996).

12. S. Bhargava, Ph.D. dissertation, University of California at Santa Barbara, December 1998.

13. S.-H. Wei and A. Zunger, Appl. Phys. Lett. **56,** 662 (1990).

14. S.-H. Wei, D. B. Laks, and A. Zunger, Appl. Phys. Lett. **62,** 1937 (1993).

15. Y. Zhang, A. Mascarenhas, P. Ernst, F. A. J. M. Driessen, D. J. Friedman, C. Geng, F. Scholz, and H. Schweizer, J. Appl. Phys. **81,** 6365 (1997).

16. M. C. DeLong, D. J. Mowbray, R. A. Hogg, M. S. Skolnick, J. E. Williams, K. Meehan, S. R. Kurtz, J. M. Olson, R. P. Schneider, M. C. Wu, and M. Hopkinson, Appl. Phys. Lett. **66,** 3185 (1995).

17. P. Ernst, C. Geng, F. Scholz, H. Schweizer, Y. Zhang, and A. Mascarenhas, Appl. Phys. Lett. **67,** 2347 (1995).

18. B. T. McDermott, K. G. Reid, N. A. El-Masry, S. M. Bedair, W. M. Duncan, X. Yin, and F. H. Pollak, Appl. Phys. Lett. **56,** 1172 (1990).

19. J. J. O'Shea, C. M. Reaves, S. P. DenBaars, M. A. Chin, and V. Narayanamurti, Appl. Phys. Lett. **69,** 3022 (1996).

20. M. Kozhevnikov, V. Narayanamurti, A. Mascarenhas, Y. Zhang, J.M. Olson, and D. L. Smith, Appl. Phys. Lett **75,** 1128 (1999).

21. G. B. Stringfellow and G. S. Chen, J. Vac. Sci. Technol. B **9,** 2182 (1991).

22. D. J. Friedman, J. G. Zhu, A. E. Kibber, J. M. Olson, and J. Moreland, Appl. Phys. Lett. **63,** 1774 (1993).

23. S. R. Kurtz, J. Appl. Phys. **74,** 4130 (1993).

24. S. H. Kwok, P. Y. Yu, and K. Uchida, Phys. Rev. B **58,** R13395 (1998).

25. T. Kippenberg, J. Krauss, J. Spieler, P. Kiesel, G. H. Dohler, R. Stubner, R. Winkler, O. Pankratov, and M. Moser, Phys. Rev. B **60,** 4446 (1999).

26. A. Zunger, private communications.

27. S.-H. Wei, A. Franceschetti, and A. Zunger, Phys. Rev. B **51,** 13 097 (1995).

28. F. Hatami, N. N. Ledentsov, M. Grundmann, J. Bohrer, F. Heinrichsdorff, M. Beer, D. Bimberg, S. S. Ruvimov, P. Werner, U. Gosele, J. Heydenreich, U. Richter, S. V. Ivanov, B. Y. Meltser, P. S. Kop'ev, and A. P. L. Zh. I. Alferov, 656 (1995)., Appl. Phys. Lett. **67,** 656 (1995).

29. B. R. Bennett, R. Magno, and B. V. Shanabrook, Appl. Phys. Lett. **68,** 505 (1996).

30. C.-K. Sun, G. Wang, J. E. Bowers, B. Brar, H.-R. Blank, H. Kroemer, and M. H. Pilkuhn, Appl. Phys. Lett. **68,** 1543 (1996).

31. D. L. Smith and S. M. Kogan, Phys. Rev. B **54,** 10354 (1996).

32. M. E. Rubin, H. R. Blank, M. A. Chin, H. Kroemer, and V. Narayanamurti, Appl. Phys. Lett. **70,** 1590 (1997).

33. S. D. Lester, F. A. Ponce, M. G. Craford, and D. A. Steigerwald, Appl. Phys. Lett. **66,** 1249 (1995).

34. E. Brazel, M. A. Chin, and V. Narayanamurti, Appl. Phys. Lett. **74,** 2367 (1999).

35. S. Bhargava, C. Zheng, J. Ko, M. A. Chin, L. A. Coldren, and V. Narayanamurti, Appl. Phys. Lett. **73,** 3271 (1998).

36. S. Bhargava, H.-R. Blank, E. Hall, M. A. Chin, H. Kroemer, and V. Narayanamurti, Appl. Phys. Lett. **74,** 1135 (1999).

VIII. Interactions and Transition

During the period of the AFOSR a large number of publications have resulted (see below). In addition the work has been presented in Invited Talks at several major conferences (APS, MRS. SPIE and WOFE-99) and numerous seminars at major universities and national laboratories. The early BEEM work involved collaboration with Surface/Interface Inc. of Mountain View, California and subsequently a collaboration was developed with Digital Instruments in Santa Barbara, California.

PhD Theses

"Local Electrical Transport Studies of Individual Self-Assembled Quantum Dots using BEEM," M. Rubin, PhD Thesis in Physics, UCSB, May 1998.

"BEEM Studies of Heterojunciton Offsets and Dislocations in Buried Semiconductor Structures," S. Bhargava, PhD Thesis in Electrical Engineering, UCSB, August 1998.

Publications

1. "Atomic and mesoscopic-scale characterization of semiconductor interfaces by ballistic-electron-emission microscopy," E.Y. Lee, S. Bhargava, M. A. Chin, and V. Narayanamurti, Invited Paper, AVS Annual Meeting, Philadelphia, October 1996; *JVST A* **15** (3) 1351-1357 (1997).

2. "The role of BEEM for characterization of physical phenomena in semiconductors alloys and quantum structures," V. Narayanamurti and M. Kozhevnikov, Invited Review Paper to be published in the *International Journal of High Speed Electronics and Systems* (submitted 1999).
3. "Fermi Level Pinning Position at the Au-InAs Interface Determined using Ballistic Electron Emission Microscopy ,"
   S. Bhargava, H.R. Blank, V. Narayanamurti, and H. Kroemer, *Appl. Phys. Lett.* **70** (6) 759 (1997).
4. "Local Conduction Band Offset of GaSb Self Assembled Quantum Dots on GaAs," M.E. Rubin, H.R. Blank, M.A. Chin,
   H. Kroemer, and V. Narayanamurti, *Appl. Phys. Lett.* **70** (12), 1590-1592 (1997).
5. "Ballistic Electron Emission Spectroscopy of $Al_XGa_{1-X}As$/GaAs Heterostructures: Conduction Band Offsets, Transport Mechanisms, and Band Structure Effects," J.J. O'Shea, E.G. Brazel, M.E. Rubin, S. Bhargava, M.A. Chin, and V. Narayanamurti, *Phys. Rev.* ***B 56*** (3) 2026-2035 (1997).
6. "Ballistic Electron Emission Microscopy (BEEM) and Spectroscopy of Buried Semiconductor Heterostructures and Quantum Dots," V. Narayanamurti, *Sci. Rep. RITU* **A44** (2), 165-172 (1997).
7. "Monte Carlo Simulations of ballistic-electron-emission-microscopy imaging and spectroscopy of buried mesoscopic structures," E.Y. Lee, V. Narayanamurti, and D.L. Smith, *Phys. Rev. B Rapid Communications* **55** (24) R16033-036 (1997).

8. "Theory of Ballistic Electron Emission Microscopy Nonepitaxial Metal/Semiconductor Interfaces," D.L. Smith, E.Y. Lee, and V. Narayanamurti, *Phys. Rev. Lett.* **80** (11), 2433-2436 (1998).
9. "Al(As,Sb) Heterobarriers on InAs: Growth, Structural Properties, and Electrical Transport," H.-R. Blank, S. Mathis, E. Hall, S. Bhargava, A. Behres, M. Henken, H. Kroemer, and V. Narayanamurti, *J. Crystal Growth* **187**, 18-28 (1998).
10. "Ballistic-electron-emission microscopy of semiconductor heterostructures," L. D. Bell, and V. Narayanamurti, *Current Opinion in Solid State & Materials Science.* **3** (1), 38-43 (1998).
11. "Scanning capacitance microscopy imaging of threading dislocations in GaN films grown on (0001) sapphire by metalorganic chemical vapor deposition," P.J. Hansen, Y.E. Strausser, A.H. Erickson, E.J. Tarsa, P.Kozodoy, E.G. Brazel, J.P. Ibbetsen, U. Mishra, V. Narayanamurti, S.P. DenBaars, and J.S. Speck, *Appl. Phys. Lett.* **72** (18), 2247-2249 (1998).
12. "Ballistic Electron Emission Microscopy (BEEM) of novel semiconductor heterostructures and quantum dots," V. Narayanamurti, Invited Paper, San Jose, CA, *SPIE Proceedings*, **3287**, 152-166, (1998).
13. "Thermoelectric Effects in Submicron Heterostructure Barriers," A. Shakouri, E.Y. Lee, D.L. Smith, V. Narayanamurti, and J.E. Bowers, *Microscale Thermophysical Engineering* **2**, 37-47 (1998).
14. "Measurement of the AlGaInAs/AlGaAs conduction band offset using Ballistic Electron Emission Spectroscopy," S. Bhargava, C. Zheng, J. Ko, M.A. Chin, L.A.Coldren, and V. Narayanamurti, *Appl. Phys. Lett.* **73**, 3271 (1998).
15. "Imaging and local transport measurements of GaSb self-assembled quantum dots on GaAs," M.E. Rubin, H.-R Blank, M.A. Chin, H. Kroemer, V. Narayanamurti, *Physica E* **2**, 682-684 (1998)
16. "Staggered to straddling band lineups in InAs/Al(As,Sb)," S. Bhargava, H.-R. Blank, E.Hall, M.A. Chin, H. Kroemer, and V. Narayanamurti, *Applied Physics Letters* **74**, 1135 (1999).
17. "Direct observation of localized high current densities in GaN films," E. Bräzel, M.A. Chin, and V. Narayanamurti, *Appl. Phys. Lett.* **74**, 2367 (1999).
18. "Effect of Electron Scattering on Second Derivative Ballistic Electron Emission Spectroscopy in Au/GaAs/AlGaAs Heterostructures," M. Kozhevnikov, V. Narayanamurti, C. Zheng, Yi-Jen Chiu, and D.L. Smith, *Phys. Rev. Lett.* **82**, 3677 (1999).
19. "Ordering-induced band structure effects in $GaInP_2$ studied by Ballistic Electron Emission Spectroscopy," M. Kozhevnikov, V. Narayanamurti, A. Mascarenhas, Y. Zhang, J.M. Olson and D.L. Smith, *App. Phys. Lett.* **75**, 1128 (1999).
20. "Scattering Theory of Ballistic Electron Emission Microscopy at Nonepitaxial Interfaces," D.L. Smith, M. Kozhevnikov, E.Y. Lee, and V. Narayanamurti, *Phys. Rev. B* **.61,** 13 914 (2000).
21. "The role of BEEM for characterization of physical phenomena in semiconductors alloys and quantum structures," V. Narayanamurti and M. Kozhevnikov, Invited Review Paper to be published in the *International Journal of High Speed Electronics and Systems* (In press 2000).

SUMMARY

Over the years of AFOSR support, we have successfully developed Ballistic Electron Emission Microscopy (BEEM) as a powerful low energy electron spectroscopy technique for probing nanometer size electronic objects and defects. The work has been widely published and disseminated.